



Reevaluation of EISCAT plasma parameters during the May 2024 geomagnetic storm using O^+ ratios from AMIE-driven SD-WACCM-X

Florian Günzkofer¹, Anders Tjulin², Gang Lu³, Hanli Liu³, and Gunter Stober^{4,5}

¹Institute for Solar-Terrestrial Physics, German Aerospace Center (DLR), Neustrelitz, Germany

²EISCAT AB, Kiruna, Sweden

³High Altitude Observatory, National Center for Atmospheric Research, Boulder, CO, USA

⁴Institute of Applied Physics, Microwave Physics, University of Bern, Bern, Switzerland

⁵Oeschger Center for Climate Change Research, Microwave Physics, University of Bern, Bern, Switzerland

Correspondence: Florian Günzkofer (florian.guenzkofer@dlr.de)

Abstract. We present a reevaluation of EISCAT plasma parameters during the May 2024 geomagnetic storm, applying the ion composition from an AMIE-driven SD-WACCM-X simulation instead of the standard IRI model. This resulted in significant deviations of F1 region electron densities (up to 15%), electron temperature (40%), and ion temperatures (30%) from the original analysis. Basic correlations of plasma parameter deviations and differences in ion composition indicate the possibility of deriving a correction model if the presented approach is extended to a large measurement database. Parameter uncertainties are also shown to be affected by the reevaluation (5% - 10%), and the general relations of parameter uncertainty, ion composition differences, and absolute ion composition profiles are investigated. It is shown that in the F1 region, the plasma parameter deviations are notably larger than the uncertainty range. Incorrect assumptions about the ion composition can have a significant impact on the accuracy of ISR measurements, and that has important consequences for the possible application of ISR data in data assimilation. Advantages and disadvantages compared to previously presented approaches regarding the ion composition issue are discussed. The main advantage of the presented method is that the physics-based background enables debiasing of EISCAT plasma parameters from standard analysis.

1 Introduction

Incoherent Scatter Radar (ISR) measurements are a crucial component of many space weather studies, as they provide multiple ionosphere parameters, including electron density, ion/electron temperature, and ion velocity. However, these parameters are inferred from the incoherent scatter spectrum, assuming certain *a priori* parameters, most notably the ratio of atomic oxygen ion (O^+) density to the electron density, N_e . It has been shown in the past that the assumed ion composition has a considerable effect on the electron and ion temperature measurements (e.g., Blelly et al., 2010; Zettergren et al., 2011; Martínez-Ledesma and Díaz Quezada, 2019; Virtanen et al., 2021; Günzkofer et al., 2025b). Hence, the measurement reliability is strongly affected by the accuracy of the *a priori* modeled O^+ ratio profile.

The most commonly applied empirical ionosphere model is the International Reference Ionosphere (IRI, Rawer et al., 1978).



Bilitza et al. (2022) gives an overview of the different IRI versions and applied parameterizations. They note that the accuracy of empirical ion composition models is significantly limited by the scarcity of measurements, especially for statistically rare conditions, e.g., during geomagnetic storms. Physics-based thermosphere-ionosphere models obtain the ion composition by solving the continuity and momentum equations of the ionosphere (Sojka, 1989). However, though the ion chemistry in the F region is considerably simpler than in the D and E regions (Rishbeth and Garriott, 1969), plasma dynamics and thermosphere-ionosphere coupling affect the accuracy of the modeled ion composition (e.g., Zettergren et al., 2010; Huba et al., 2021; Lee et al., 2024). Nevertheless, physics-based ionosphere models are likely to cover the variability of the F region ion composition better than empirical models for geomagnetically active periods.

We reevaluate the ISR measurements with the EISCAT Svalbard Radar during the major geomagnetic storm in May 2024 (Themens et al., 2024). For this reevaluation, we replace the O^+ ratios given by the default ionosphere *a priori* model (IRI2020) of the EISCAT analysis with the O^+ ratios as given by the physics-based Whole Atmosphere Community Climate Model with thermosphere/ionosphere extension (WACCM-X). Different high-latitude drivers of the WACCM-X model are compared.

Section 2 gives an overview of the applied measurements and models. Section 3 shows the reevaluated plasma parameters and relates them to the model differences in O^+ ratio. Section 4 discusses the obtained results, and the advantages and disadvantages of the technique applied in this paper compared to previous solutions of the ion composition issue. Section 5 summarizes the main conclusion and gives an outlook on future work.

2 Measurements and models

2.1 EISCAT Svalbard Radar

The EISCAT Svalbard Radar (ESR) is located at 78.2°N , 16.1°E , inside the polar cusp, and has been in operation for nearly 30 years (Wannberg et al., 1997; Baddeley et al., 2023). It operates at a radar frequency of 500 MHz and consists of two parabolic receive antennas: one fully steerable with a 32 m diameter and one fixed along the local geomagnetic field direction, with a 42 m diameter. During the major geomagnetic storm in May 2024, the ESR was continuously operated from 10 May 13:00 UT to 14 May 12:00 UT in the *ipy_fixed42m* mode. This means that only the 42 m antenna was utilized and, hence, all measurements are conducted at 81.6° elevation along the local magnetic field. More information about EISCAT instruments and operation modes can be found in Tjulin (2025).

To obtain plasma parameters, EISCAT measurements are analyzed with the Grand Unified Incoherent Scatter Design and Analysis Package GUISDAP (Lehtinen and Huuskonen, 1996). We leverage the GUISDAP version 9.2 (Hägström, 2021), which includes the IRI2020 (Rawer et al., 1978; Bilitza et al., 2022) and the NRLMSIS 2.1 (Emmert et al., 2022) to generate an *a priori* state of the atmosphere-ionosphere system. The GUSIDAP sub-function, which calls the ionosphere *a priori* model, was modified to acquire the O^+ ratio from a previously prepared input file for reevaluation. The autocorrelation function of the radar signal was integrated over 300 seconds for each analysis step. This is considerably longer than the default 60-second integration period, but was chosen to match the output frequency of the whole-atmosphere model (see Section 2.2).



2.2 SD-WACCM-X

55 WACCM-X is a whole-atmosphere model developed and maintained by the National Center for Atmospheric Research (Liu et al., 2018). SD-WACCM-X is the *specified dynamics* model configuration, which means that lower atmosphere dynamics are nudged to the MERRA2 reanalysis (Rienecker et al., 2011). SD-WACCM-X has been validated and applied in multiple previous studies (e.g., Stober et al., 2021; Hindley et al., 2022; Günzkofer et al., 2022; Shi et al., 2025).

The model run applied for the present study was conducted at approximately $1.9^\circ \times 2.5^\circ$ latitude-longitude and 0.25 scale
60 heights vertical resolution. Instantaneous outputs of the basic atmosphere-ionosphere parameters, including the ion composition, were written in 5-minute intervals to obtain a maximum time resolution while keeping the computational cost and data amount reasonable.

Specifying the geomagnetic forcing of thermosphere-ionosphere models is an important issue, since it has been shown that different models for the high-latitude electrodynamics result in considerably different thermosphere-ionosphere conditions
65 (Günzkofer et al., 2024, 2025a). The "default" choice is empirical models of the high-latitude convection pattern. However, data assimilative methods are generally considered to result in a more realistic geomagnetic forcing, but are also more difficult to obtain compared to standard empirical models. We will compare the O^+ ratios from two WACCM-X runs, driven with the empirical Heelis convection model (Heelis et al., 1982) and the Assimilative Mapping of Ionospheric Electrodynamics (AMIE, Richmond and Kamide, 1988). The Heelis model applies the 3-hourly Kp index for parameterization. For the May 2024
70 superstorm, the AMIE assimilation includes measurements by the SuperDARN radar network, the SuperMAG magnetometer network, DMSP satellite measurements of ion drift, DMSP/SSUSI measurements of auroral precipitation, as well as AMPERE and Swarm (A and B) satellite magnetic field data.

3 Results

The major geomagnetic storm of May 2024 was the strongest space weather event in two decades and reached the maximum
75 possible $Kp = 9$ index. A complete overview of the storm impact at high latitudes can be found in Themens et al. (2024). It can be seen that the geomagnetic storm starts at about 17:00 UT on 10 May and reaches its maximum during the night from 10-11 May. On 11 and 12 May, Themens et al. (2024) showed a strongly pronounced negative storm phase, indicating significant thermospheric upwelling and consequent disturbances of the chemical composition at the thermosphere/ionosphere. Figure 1 shows the EISCAT ESR measurements of electron density N_e , electron temperature T_e , and ion temperature T_i from 10 - 13
80 May 2024.

As described in Section 2.1 and Günzkofer et al. (2025b), the plasma parameters in Figure 1 are inferred from the incoherent scatter spectrum assuming certain *a priori* parameters from the empirical IRI 2020 and NRLMSIS 2.1 models. Figure 2 a) shows the O^+ -to- N_e ratio r_{O^+} as given by the IRI model from 10 - 13 May 2024. It can be seen that IRI provides the diurnal variation of r_{O^+} but no variations as expected from the varying geomagnetic conditions during this period. The Heelis- and
85 AMIE-driven WACCM-X O^+ ratios in Figures 2 b) and c) show this variation of r_{O^+} with geomagnetic activity. The low r_{O^+} well up into the F region at around 08:00 UT on 11 May, presumably connected to the uplift of molecular atmospheric

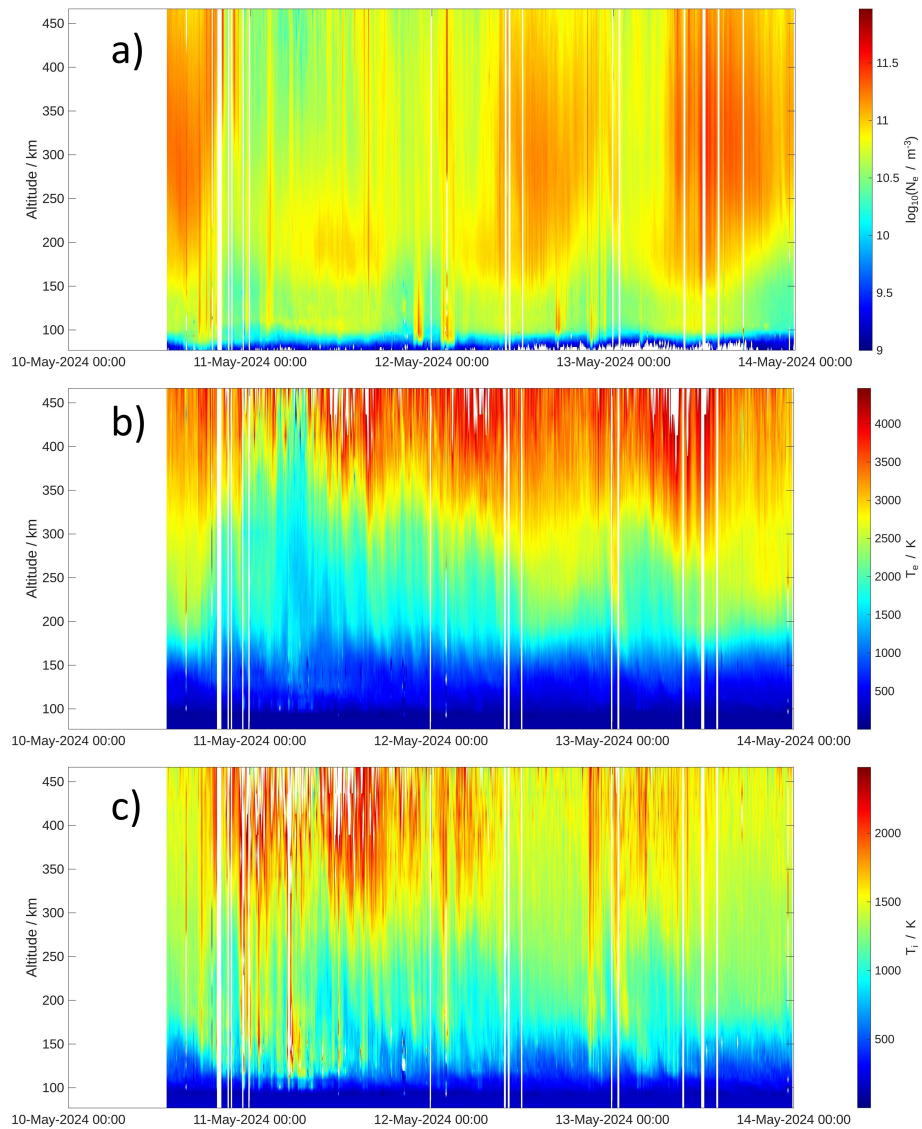


Figure 1. EISCAT ESR measurements of a) electron density, b) electron temperature, and c) ion temperature from 10 - 13 May 2024.

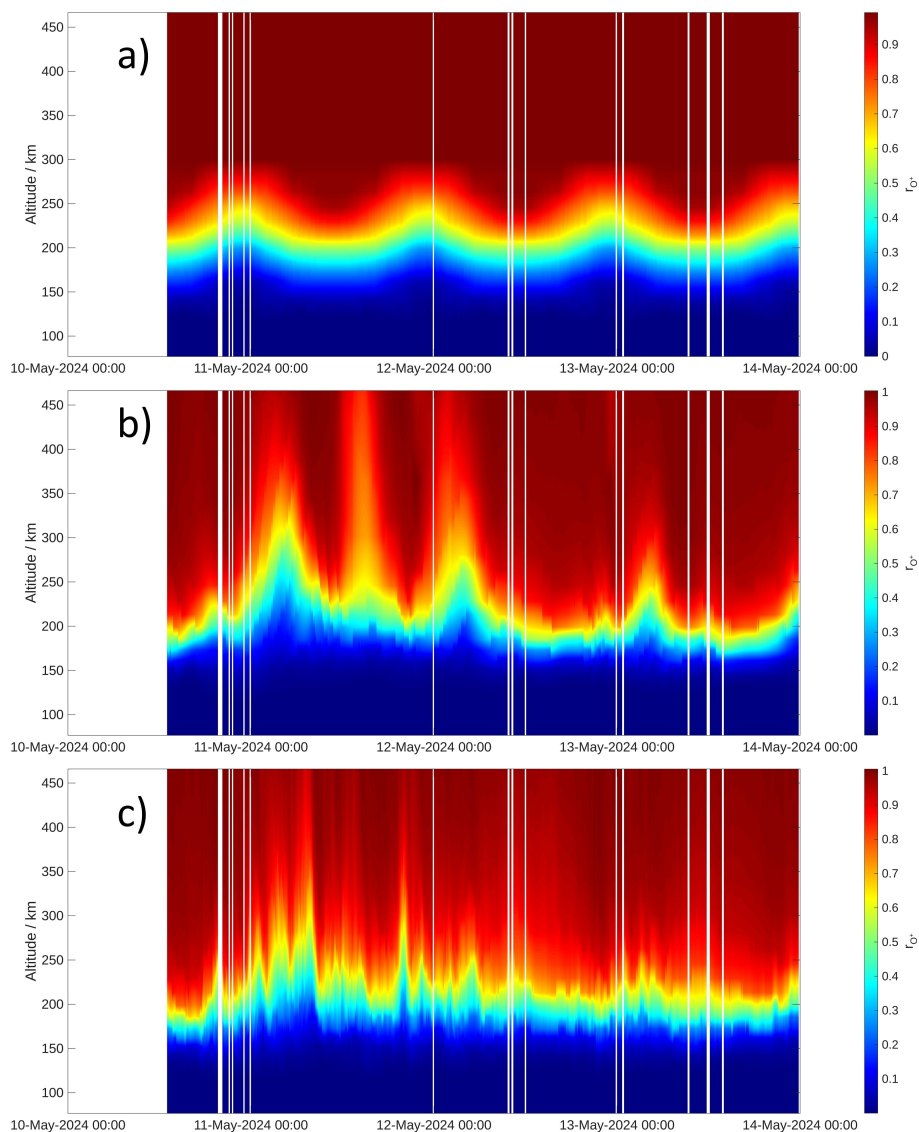


Figure 2. O^+ ratios r_{O^+} given by a) the IRI 2020 model, b) the Heelis-driven, and c) the AMIE-driven WACCM-X runs.

constituents following the main phase of the storm, can be seen in both WACCM-X runs. However, the variability of r_{O^+} is distinctly lower in the Heelis-driven model run, as expected due to the driving with the 3-hourly Kp index. Since the data assimilative AMIE method is expected to cover the actual geomagnetic forcing better than the empirical Heelis model (Günzkofer et al., 2025a), the further analysis in this paper will be conducted using the AMIE-driven WACCM-X model results. Due to the limited availability of AMIE results, the Heelis-driven model r_{O^+} is presumably more widely applicable for the reevaluation of EISCAT measurements demonstrated below.



The GUSIDAP software for inferring EISCAT plasma parameters contains a subroutine *ionomodel.m* which, by default, calls upon the IRI 2020 model to give *a priori* estimates of the fitted plasma parameters as well as an *a priori* O^+ ratio that is assumed as true during the fitting of plasma parameters. We adjusted this subroutine and opened a path to directly read the O^+ ratio from the prepared WACCM-X run. The adjusted *ionomodel.m* routine as well as the WACCM-X data files for Heelis- and AMIE-driven model runs are provided in a software and data repository (Günzkofer et al., 2026). We would like to emphasize again that all results shown below are obtained by applying the AMIE-driven model results.

Figure 3 a) shows the difference of O^+ ratio Δr_{O^+} between WACCM-X and IRI during the May 2024 storm. Figures 3 b) - d) show the percentage changes

$$dX = \frac{X_{reevaluation} - X_{original}}{X_{original}} \cdot 100 \quad (1)$$

of N_e , T_e , and T_i in the reevaluation using WACCM-X r_{O^+} compared to the original EISCAT parameters. It can be seen that for all three parameters dX has a negative correlation with Δr_{O^+} . While dN_e is limited to about $\pm 10\%$ at maximum deviation, dT_i can reach up to $\pm 30\%$ and dT_e even up to $\pm 40\%$.

Figure 4 illustrates the correlation of Δr_{O^+} and dX . We distinguish two altitude regimes, above and below the transition altitude z_{50} , as applied by Virtanen et al. (2021), where half of the ionospheric plasma consists of atomic oxygen ions, i.e., $r_{O^+}(z_{50}) = 0.5$. It can be seen that the percentage change between original analysis and reevaluation is strongly negatively correlated ($R < -0.9$) in all cases, except for dN_e below the transition altitude. This indicates that in most cases, a reevaluation of the EISCAT measurements is not necessary, but a linear correction model could be derived. For the case of dT_e above z_{50} , which has the highest correlation with Δr_{O^+} , we determine a linear function $dT_e = A \cdot \Delta r_{O^+} + B$, so that

$$T_{e,reevaluated} = T_{e,o} \cdot \left(\frac{A \cdot \Delta r_{O^+}}{100} + \frac{B}{100} + 1 \right). \quad (2)$$

We find that $A = -74.8138$ and $B = 0.2261$ (hence $B/100 \ll 1$ can be neglected) for this case. However, a reliable correction model that can be applied to other EISCAT measurements would require a statistical analysis of EISCAT measurements. The idea of a correction function was already suggested by Waldteufel (1971), but the significant increase in ISR measurements since then would allow for a statistically more sound evaluation. Also, non-linear relations, as already discussed by Waldteufel (1971), should be considered. The scope of this paper is the May 2024 superstorm, but the development of such a correction model might prove useful in the future.

Figures 5 a) - c) show the analogous percentage changes of the plasma parameter uncertainties $d\delta X$. For all three parameters, the percentage change between reevaluation and the original analysis is below 10%. However, it becomes apparent that the correlation with Δr_{O^+} is not as straightforward as with dX in Figure 3.

In Figure 5, the transition altitudes given by the IRI and WACCM-X models, interpolated to EISCAT measurement altitudes, are shown as solid (WACCM-X) and dashed (IRI) lines. The percentage change of the parameter uncertainties has an opposite sign above, and below the smaller of the two compared transition altitudes, i.e., it depends on whether the altitude h is larger or smaller than $\min\{z_{50,WACCM-X}, z_{50,IRI}\}$. Table 1 summarizes the relations of Δr_{O^+} , h , and $d\delta X$.

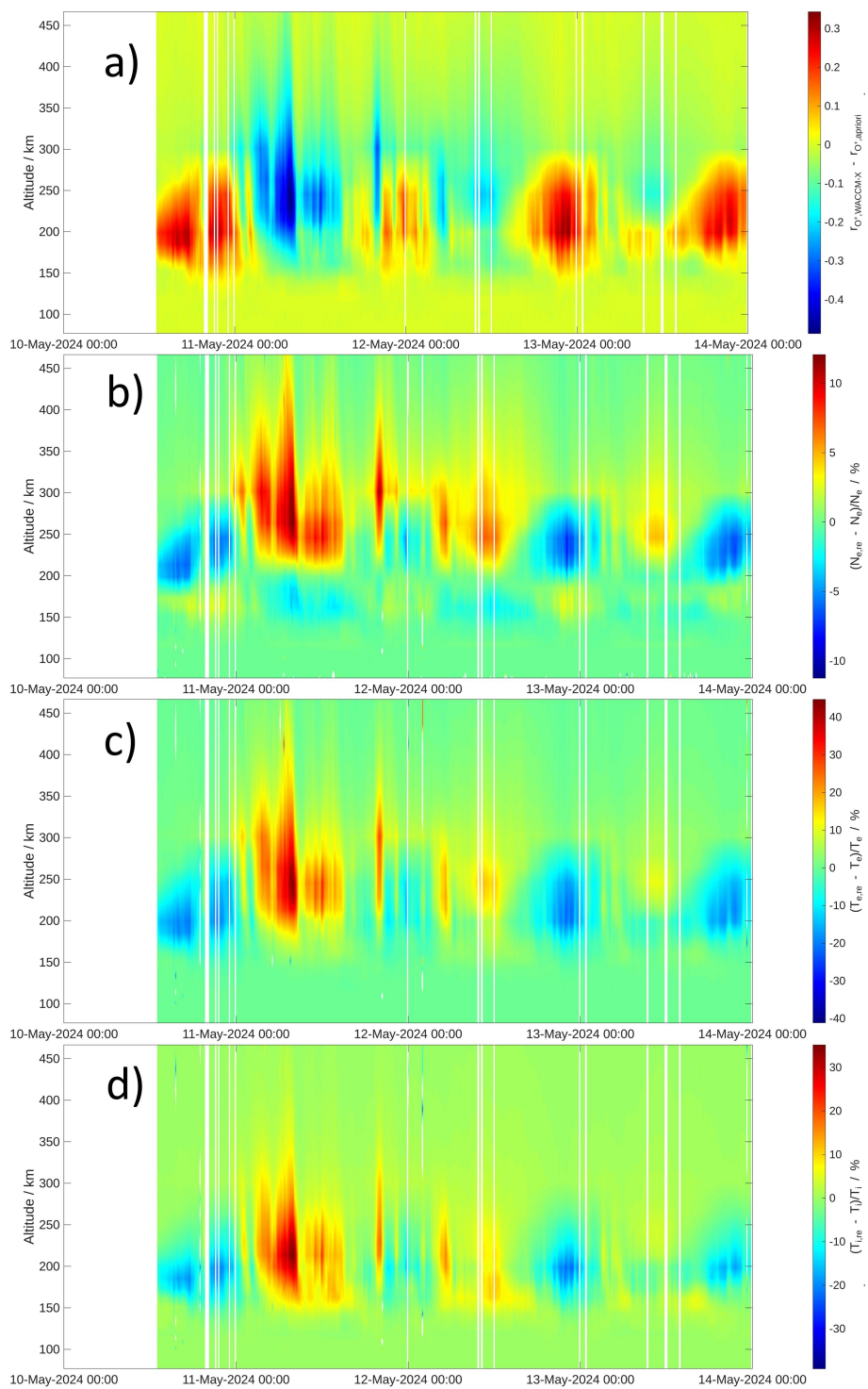


Figure 3. a) Difference of WACCM-X O^+ ratio compared to IRI. Applying the WACCM-X r_{O^+} results in reevaluated EISCAT plasma parameters $N_{e, re}$, $T_{e, re}$, and $T_{i, re}$. Figures b) - d) show the resulting percentage changes of these parameters.

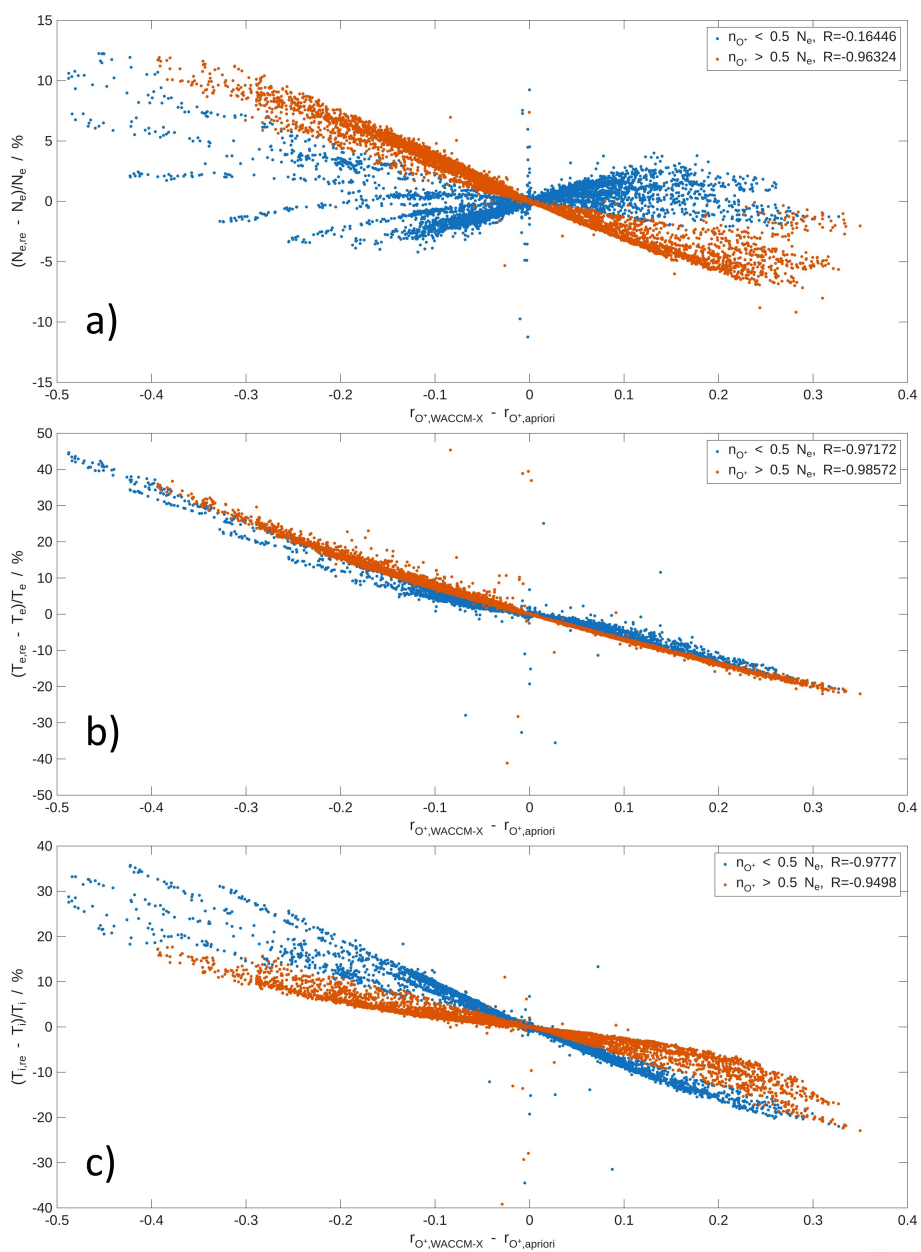


Figure 4. Correlation with Δr_{O^+} for a) dN_e , b) dT_e , and c) dT_i above and below the transition altitude.

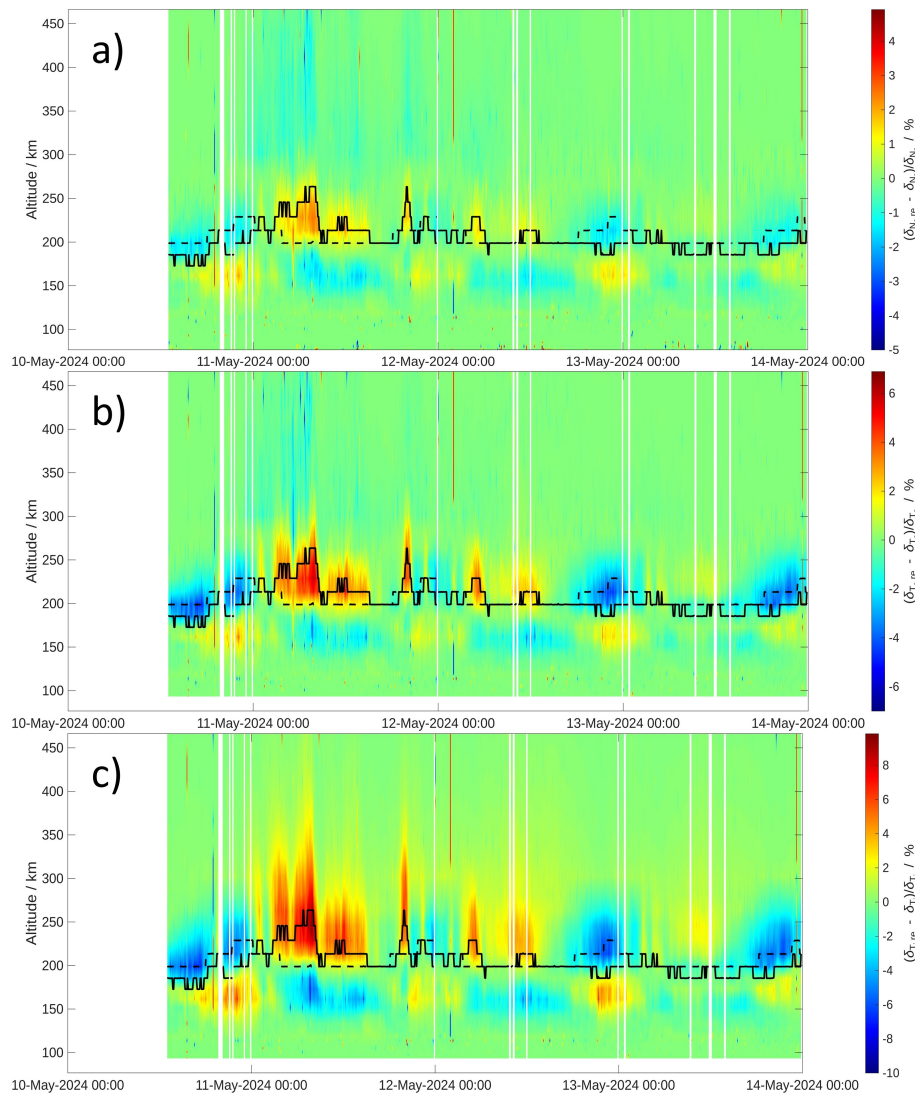


Figure 5. Percentage changes of parameter uncertainties a) δN_e , b) δT_e , and c) δT_i . Transition altitudes of $r_{O^+} = 0.5$ are shown as solid (WACCM-X) and dashed (IRI) lines.



	$\Delta r_{O^+} < 0$	$\Delta r_{O^+} > 0$
$h > \min\{z_{50,WACCM-X}, z_{50,IRI}\}$	$d\delta\mathbf{X} > 0$	$d\delta\mathbf{X} < 0$
$h < \min\{z_{50,WACCM-X}, z_{50,IRI}\}$	$d\delta\mathbf{X} < 0$	$d\delta\mathbf{X} > 0$

Table 1. Whether the plasma parameter uncertainties increase or decrease due to the reevaluation depends on the sign of Δr_{O^+} and on the altitude of the lower model z_{50} .

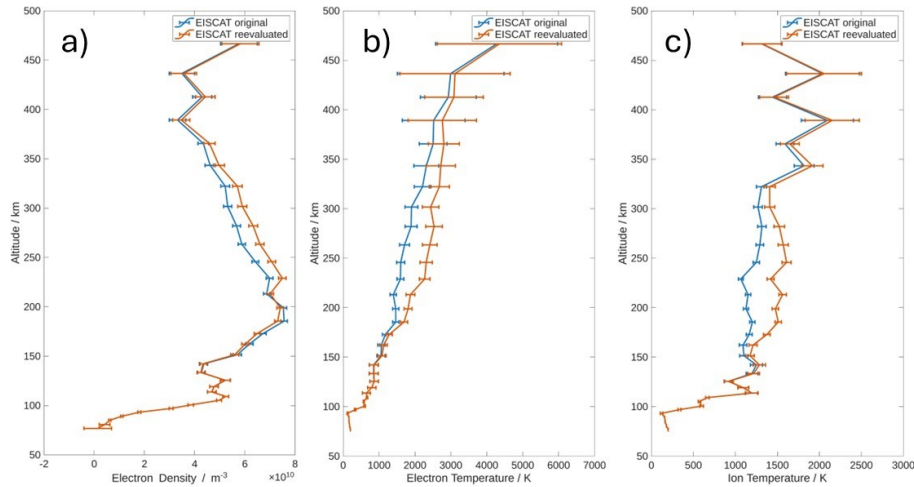


Figure 6. Vertical profiles of a) N_e , b) T_e , and c) T_i from the original EISCAT analysis and the reevaluation at 08:00 UT on 11 May 2024.

125 To obtain an impression of how the impact of the reevaluation, Figures 6 and 7 show the vertical profiles of N_e , T_e , and T_i for 11 May 08:00 UT and 12 May 22:10 UT, which are the times of minimum/maximum Δr_{O^+} respectively.

It can be seen that the deviation of the original and reevaluated profiles is mostly larger than the uncertainty range at around 200 - 300 km altitude. This demonstrates the usefulness of such a reevaluation, especially for studies investigating plasma temperatures.

130 4 Discussion

This section discusses alternative approaches to constrain/determine the O^+ ratio before or during the analysis process, in addition to the default GUSIDAP analysis, using IRI r_{O^+} , and the WACCM-X-based reevaluation presented in this paper. The advantages and disadvantages of each method will be compared.

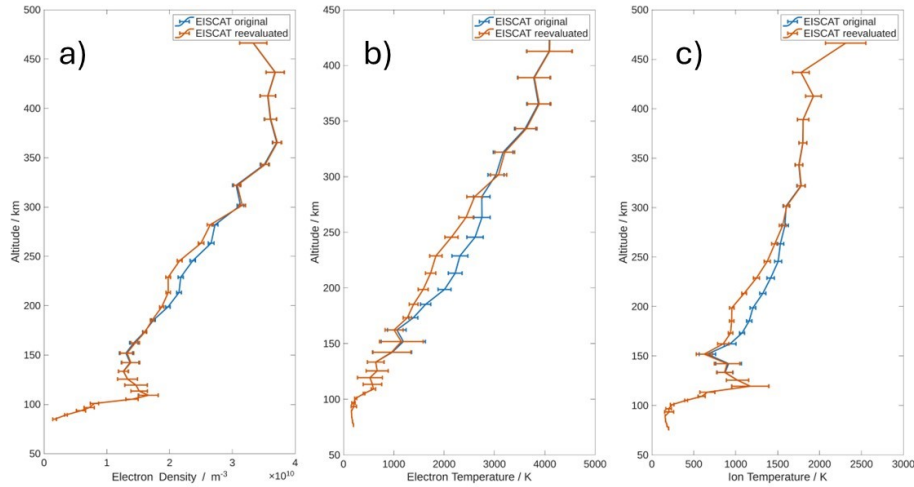


Figure 7. Same as Figure 6 but for 22:10 UT on 12 May 2024.

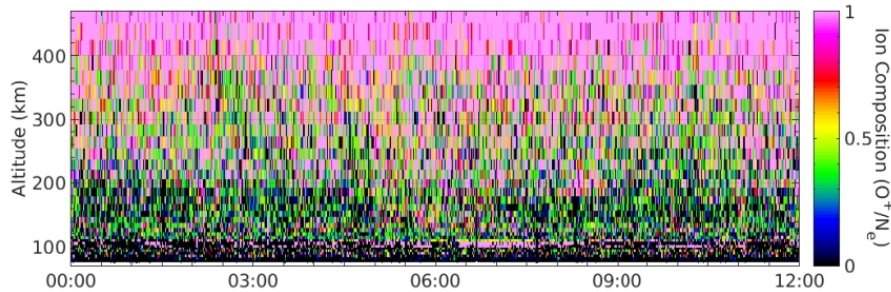


Figure 8. GUISDAP fit of O^+ ratio without constraining any other parameters on 12 May 2024 (0 - 12 UT).

4.1 Direct fitting of O^+ ratios

135 The GUISDAP software package allows for determining r_{O^+} during the analysis process without constraining it to the *a priori*
 profile. However, this results in a very noisy r_{O^+} , as shown in Figure 8, and consequently large uncertainties of all inferred
 parameters.

This issue has been previously discussed in numerous publications (see Blelly et al., 2010; Zettergren et al., 2011, and refer-
 ences therein), and alternative approaches have been discussed. Introducing a correction function, as suggested by Waldteufel
 140 (1971) and in Equation 2 has the advantage of not requiring a time-consuming reevaluation of the incoherent scatter measure-
 ments. The problem with this approach is that r_{O^+} is still assumed to be known somehow (in our case, from AMIE/WACCM-X
 instead of IRI).

Blelly et al. (2010) suggested a complete reparameterization of the incoherent scatter analysis. This method allows inferring the
 standard ISR plasma parameters as well as r_{O^+} from the incoherent scatter spectrum. However, multiple assumptions about



145 the shape of r_{O^+} and the ionospheric temperatures are applied to obtain the additional parameter. Oliver (1975) derived an altitude profile for the O^+ ratio

$$r_{O^+}(h) = \frac{2}{1 + \sqrt{1 + \exp\left(-\frac{h-z_{50}}{H}\right)}} \quad (3)$$

based on the transition altitude z_{50} and a scale height parameter H for the thickness of the transition. Zettergren et al. (2011) applied Equation 3 with a constant H for further simplification they deemed justified (Zettergren et al., 2010) while Blley et al. (2010) implemented an asymmetric profile with different H^+ and H^- above and below z_{50} .

The above-described approaches provide self-consistent measurements of the ionospheric composition together with the standard ISR plasma parameters. However, the required modification of the incoherent scatter analysis limits their applicability, and the applied assumptions on the r_{O^+} profile and the ionospheric temperatures provide additional uncertainty (e.g., Equation 3 was specifically derived for mid-latitudes). The method suggested in this paper, together with the correction-function approach from Waldteufel (1971), is easily applicable, and the only, though major, assumption is the reliability of WACCM-X ion compositions. Its main use can therefore be seen as a "quick correction" for cases where IRI ion composition is presumably erroneous (e.g., during strong storm events).

4.2 Bayesian Fitting Module

Another possible approach is the Bayesian Filtering Module (BAFIM) developed by Virtanen et al. (2021). BAFIM is a full-profile fitting technique that allows inferring the four standard ISR plasma parameters at high time and altitude resolution from a multi-step fitting process. Since the full-profile fitting approach, other than the standard gate-by-gate analysis, allows for enforcing certain conditions on the parameter profiles, the ion composition can be fitted as an additional fifth parameter. The five-parameter BAFIM analysis in (Virtanen et al., 2021) was able to eliminate the artificial temperature maximum in the F1 region that is often observed in ISR measurements under erroneous r_{O^+} assumptions (Günzkofer et al., 2025b). In Virtanen et al. (2024), the BAFIM was coupled to an ion chemistry model (Richards et al., 2010; Reimer et al., 2021), providing even more reliable ion composition fits in an approach similar to the one applied in the AMISR radars (Richards et al., 2010).

The Bayesian Filtering Module, in combination with the GUISDAP software, provides the presumably most reliable method for inferring EISCAT plasma parameters and "correct" ion compositions. Since the main challenge is the sparse availability of ion composition measurements in the F1 region, a thorough validation is difficult. An additional problem of full-profile techniques is the large computational weight, though BAFIM avoids this issue by partially applying gate-by-gate analysis (Virtanen et al., 2021). Nevertheless, many users of EISCAT measurements do not conduct the incoherent scatter analysis themselves but rely on data products provided by the EISCAT database. Especially for these users, a simple and quick, if less accurate, correction function, as suggested in this paper, is presumably more applicable. The differences in plasma parameters shown in Virtanen et al. (2021) compare well with the deviations we obtained in Section 3, considering that the results in this paper are obtained for an extreme geomagnetic storm.



5 Conclusions and Outlook

A reevaluation of EISCAT plasma parameters during the May 2024 geomagnetic storm was conducted, assuming O^+ ratios from an AMIE-driven SD-WACCM-X run. We showed that under extreme storm conditions, the EISCAT electron density measurements deviate up to 15% compared to the standard analysis assuming IRI O^+ ratios. Electron and ion temperatures were shown to deviate even stronger, up to 40% and 30%, respectively. We showed a very high linear correlation of electron temperature deviations and r_{O^+} in the applied *a priori* models, opening the possibility to introduce a simple correction function. The uncertainties in the plasma parameters were impacted by the reevaluation, increasing by about 5% to 10%. However, whether the uncertainty is increased or decreased due to the reevaluation depends on the transition altitudes of the two *a priori* models. However, the deviations of F1 region plasma parameters between the original analysis and reevaluation are notably larger than the uncertainty range.

As discussed in Section 4, the main advantage of an ISR measurement reevaluation based on the ion composition given by a physics-based thermosphere-ionosphere model is the possibility to extend the method into a correction model. Due to the limited availability of AMIE results coinciding with EISCAT measurements, a correction model would have to be based on standard high-latitude drivers of WACCM-X, i.e., the Heelis and Weimer empirical convection models. Such a correction model would be quickly and easily applicable to all researchers, regardless of their proficiency with incoherent scatter analysis software.

Code and data availability. The data and software required to reproduce the shown results are available under the Creative Commons Attribution 4.0 International license at <https://doi.org/10.5281/zenodo.18599344> (Günzkofer et al., 2026).

Author contributions. FG conducted the formal analysis and wrote the original manuscript draft. AT assisted with and validated the modified GUISDAP analysis and conducted the GUISDAP O^+ fit in Section 4. GL generated and provided the AMIE input files for the May 2024 storm. HL assisted with the WACCM-X model runs. GS supervised the project and wrote parts of the manuscript. All authors were involved in revising the final manuscript.

Competing interests. At least one of the co-authors is a handling editor at *Annales Geophysicae*.

Acknowledgements. We acknowledge the support of EISCAT AB, a not-for-profit company operating research radars funded by research organisations in Finland (RCF), Japan (NIPR and ISEE), Norway (NFR), Sweden (VR), and the United Kingdom (UKRI). The National Center for Atmospheric Research is a major facility sponsored by the National Science Foundation under Cooperative Agreement 1852977.

<https://doi.org/10.5194/egusphere-2026-823>
Preprint. Discussion started: 25 February 2026
© Author(s) 2026. CC BY 4.0 License.



Gunter Stober is a member of the Oeschger Center for Climate Change Research (OCCR). The internal pre-review at DLR-SO by Hiroatsu Sato is gratefully acknowledged.



References

- 205 Baddeley, L., Lorentzen, D., Haaland, S., Heino, E., Mann, I., Miloch, W., Oksavik, K., Partamies, N., Spicher, A., and Vierinen, J.: Space and atmospheric physics on Svalbard: a case for continued incoherent scatter radar measurements under the cusp and in the polar cap boundary region, *Progress in Earth and Planetary Science*, 10, 53, <https://doi.org/10.1186/s40645-023-00585-9>, 2023.
- Bilitza, D., Pezzopane, M., Truhlik, V., Altadill, D., Reinisch, B. W., and Pignalberi, A.: The International Reference Ionosphere Model: A Review and Description of an Ionospheric Benchmark, *Reviews of Geophysics*, 60, e2022RG000792, <https://doi.org/10.1029/2022RG000792>, 2022.
- 210 Bletly, P.-L., Alcaydé, D., and van Eyken, A. P.: A new analysis method for determining polar ionosphere and upper atmosphere characteristics from ESR data: Illustration with IPY period, *Journal of Geophysical Research (Space Physics)*, 115, A09322, <https://doi.org/10.1029/2009JA014876>, 2010.
- Emmert, J. T., Jones, M., Siskind, D. E., Drob, D. P., Picone, J. M., Stevens, M. H., Bailey, S. M., Bender, S., Bernath, P. F., Funke, B., Hergig, M. E., and Pérot, K.: NRLMSIS 2.1: An Empirical Model of Nitric Oxide Incorporated Into MSIS, *Journal of Geophysical Research (Space Physics)*, 127, e2022JA030896, <https://doi.org/10.1029/2022JA030896>, 2022.
- 215 Günzkofer, F., Pokhotelov, D., Stober, G., Liu, H., Liu, H. L., Mitchell, N. J., Tjulin, A., and Borries, C.: Determining the Origin of Tidal Oscillations in the Ionospheric Transition Region With EISCAT Radar and Global Simulation Data, *Journal of Geophysical Research (Space Physics)*, 127, e2022JA030861, <https://doi.org/10.1029/2022JA030861>, 2022.
- 220 Günzkofer, F., Liu, H., Stober, G., Pokhotelov, D., and Borries, C.: Evaluation of the Empirical Scaling Factor of Joule Heating Rates in TIE-GCM With EISCAT Measurements, *Earth and Space Science*, 11, e2023EA003447, <https://doi.org/10.1029/2023EA003447>, 2024.
- Günzkofer, F., Liu, H., Liu, H., Stober, G., Lu, G., Wu, H., Bartel, N., Heymann, F., and Borries, C.: High-Latitude Joule Heating in TIE-GCM 3.0: Evaluation of Different Plasma Convection Forcing Models, , 52, e2025GL117647, <https://doi.org/10.1029/2025GL117647>, 2025a.
- 225 Günzkofer, F., Stober, G., Heymann, F., Tjulin, A., and Borries, C.: Altitude-Dependent Plasma Parameter Variations of Synthetic EISCAT UHF and VHF Incoherent Scatter Spectra Calculated From TIE-GCM Results, *Journal of Geophysical Research (Space Physics)*, 130, 2024JA033471, <https://doi.org/10.1029/2024JA033471>, 2025b.
- Günzkofer, F., Tjulin, A., Liu, H., Lu, G., and Stober, G.: [Data& Software] Reevaluation of EISCAT plasma parameters during the May 2024 geomagnetic storm using O+ ratios from AMIE-driven SD-WACCM-X, <https://doi.org/10.5281/zenodo.18599344>, 2026.
- 230 Häggström, I.: Guisdap9, <https://gitlab.com/eiscat/guisdap9>, 2021.
- Heelis, R. A., Lowell, J. K., and Spiro, R. W.: A model of the high-latitude ionospheric convection pattern, *Journal of Geophysical Research*, 87, 6339–6345, <https://doi.org/10.1029/JA087iA08p06339>, 1982.
- Hindley, N. P., Mitchell, N. J., Cobbett, N., Smith, A. K., Fritts, D. C., Janches, D., Wright, C. J., and Moffat-Griffin, T.: Radar observations of winds, waves and tides in the mesosphere and lower thermosphere over South Georgia island (54° S, 36° W) and comparison with WACCM simulations, *Atmospheric Chemistry and Physics*, 22, 9435–9459, <https://doi.org/10.5194/acp-22-9435-2022>, 2022.
- 235 Huba, J. D., Heelis, R., and Maute, A.: Large Scale O⁺ Depletions Observed by ICON in the Post Midnight Topside Ionosphere: Data/Model Comparison, *Geophysical Research Letters*, 48, e92061, <https://doi.org/10.1029/2020GL092061>, 2021.
- Lee, W., Song, I.-S., Shim, J. S., Liu, G., and Jee, G.: The Impact of Lower Atmosphere Forecast Uncertainties on WACCM-X Prediction of Ionosphere-Thermosphere System During Geomagnetic Storms, *Space Weather*, 22, 2024SW004137, <https://doi.org/10.1029/2024SW004137>, 2024.
- 240



- Lehtinen, M. S. and Huuskonen, A.: General incoherent scatter analysis and GUIDAP, *Journal of Atmospheric and Terrestrial Physics*, 58, 435–452, [https://doi.org/10.1016/0021-9169\(95\)00047-X](https://doi.org/10.1016/0021-9169(95)00047-X), 1996.
- Liu, H.-L., Bardeen, C. G., Foster, B. T., Lauritzen, P., Liu, J., Lu, G., Marsh, D. R., Maute, A., McInerney, J. M., Pedatella, N. M., Qian, L., Richmond, A. D., Roble, R. G., Solomon, S. C., Vitt, F. M., and Wang, W.: Development and Validation of the Whole Atmosphere
245 Community Climate Model With Thermosphere and Ionosphere Extension (WACCM-X 2.0), *Journal of Advances in Modeling Earth Systems*, 10, 381–402, <https://doi.org/10.1002/2017MS001232>, 2018.
- Martínez-Ledesma, M. and Díaz Quezada, M. A.: Determination of the Signal Fluctuation Threshold of the Temperature-Ion Composition Ambiguity Problem Using Monte Carlo Simulations, *Journal of Geophysical Research (Space Physics)*, 124, 2897–2919, <https://doi.org/10.1029/2018JA026217>, 2019.
- 250 Oliver, W. L.: Models of F1-region ion composition variations., *Journal of Atmospheric and Terrestrial Physics*, 37, 1065–1076, [https://doi.org/10.1016/0021-9169\(75\)90152-X](https://doi.org/10.1016/0021-9169(75)90152-X), 1975.
- Rawer, K., Bilitza, D., and Ramakrishnan, S.: Goals and status of the international reference ionosphere., *Reviews of Geophysics and Space Physics*, 16, 177–181, <https://doi.org/10.1029/RG016i002p00177>, 1978.
- Reimer, A., amisr user, and Günzkofer, F.: amisr/flipchem: v2021.2.2 Bugfix Release, <https://doi.org/10.5281/zenodo.5719844>, 2021.
- 255 Richards, P. G., Bilitza, D., and Voglozin, D.: Ion density calculator (IDC): A new efficient model of ionospheric ion densities, *Radio Science*, 45, RS5007, <https://doi.org/10.1029/2009RS004332>, 2010.
- Richmond, A. D. and Kamide, Y.: Mapping electrodynamic features of the high-latitude ionosphere from localized observations: Technique, *Journal of Geophysical Research*, 93, 5741–5759, <https://doi.org/10.1029/JA093iA06p05741>, 1988.
- Rienecker, M. M., Suarez, M. J., Gelaro, R., Todling, R., Bacmeister, J., Liu, E., Bosilovich, M. G., Schubert, S. D., Takacs, L., Kim, G.-K.,
260 Bloom, S., Chen, J., Collins, D., Conaty, A., da Silva, A., Gu, W., Joiner, J., Koster, R. D., Lucchesi, R., Molod, A., Owens, T., Pawson, S., Pegion, P., Redder, C. R., Reichle, R., Robertson, F. R., Ruddick, A. G., Sienkiewicz, M., and Woollen, J.: MERRA: NASA's Modern-Era Retrospective Analysis for Research and Applications, *Journal of Climate*, 24, 3624–3648, <https://doi.org/10.1175/JCLI-D-11-00015.1>, 2011.
- Rishbeth, H. and Garriott, O. K.: *Introduction to ionospheric physics*, Academic Press, Inc., 1969.
- 265 Shi, G., Liu, H., Tsutsumi, M., Gulbrandsen, N., Kozlovsky, A., Pokhotelov, D., Lester, M., Jacobi, C., Wu, K., and Stober, G.: New insights into the polar ozone and water vapor, radiative effects, and their connection to the tides in the mesosphere–lower thermosphere during major sudden stratospheric warming events, *Atmospheric Chemistry and Physics*, 25, 9403–9430, <https://doi.org/10.5194/acp-25-9403-2025>, 2025.
- Sojka, J. J.: Global scale, physical models of the F region ionosphere., *Reviews of Geophysics*, 27, 371–403, <https://doi.org/10.1029/RG027i003p00371>, 1989.
- 270 Stober, G., Kuchar, A., Pokhotelov, D., Liu, H., Liu, H.-L., Schmidt, H., Jacobi, C., Baumgarten, K., Brown, P., Janches, D., Murphy, D., Kozlovsky, A., Lester, M., Belova, E., Kero, J., and Mitchell, N.: Interhemispheric differences of mesosphere-lower thermosphere winds and tides investigated from three whole-atmosphere models and meteor radar observations, *Atmospheric Chemistry & Physics*, 21, 13 855–13 902, <https://doi.org/10.5194/acp-21-13855-2021>, 2021.
- 275 Themens, D. R., Elvidge, S., McCaffrey, A., Jayachandran, P. T., Coster, A., Varney, R. H., Galkin, I., Goodwin, L. V., Watson, C., Maguire, S., Kavanagh, A. J., Zhang, S.-R., Goncharenko, L., Bhatt, A., Dorrian, G., Groves, K., Wood, A. G., and Reid, B.: The High Latitude Ionospheric Response to the Major May 2024 Geomagnetic Storm: A Synoptic View, , 51, e2024GL111677, <https://doi.org/10.1029/2024GL111677>, 2024.



- Tjulin, A.: EISCAT Experiments, <https://doi.org/10.5281/zenodo.15863865>, 2025.
- 280 Virtanen, I. I., Tesfaw, H. W., Roininen, L., Lasanen, S., and Aikio, A.: Bayesian Filtering in Incoherent Scatter Plasma Parameter Fits, *Journal of Geophysical Research (Space Physics)*, 126, e28700, <https://doi.org/10.1029/2020JA028700>, 1002/essoar.10504337.3, 2021.
- Virtanen, I. I., Tesfaw, H. W., Aikio, A. T., Varney, R., Kero, A., and Thomas, N.: F₁ Region Ion Composition in Svalbard During the International Polar Year 2007-2008, *Journal of Geophysical Research (Space Physics)*, 129, e2023JA032202, <https://doi.org/10.1029/2023JA032202>, 2024.
- 285 Waldteufel, P.: Combined incoherent-scatter F₁-region observations, , 76, 6995–6999, <https://doi.org/10.1029/JA076i028p06995>, 1971.
- Wannberg, G., Wolf, I., Vanhainen, L. G., Koskenniemi, K., Röttger, J., Postila, M., Markkanen, J., Jacobsen, R., Stenberg, A., Larsen, R., Eliassen, S., Heck, S., and Huuskonen, A.: The EISCAT Svalbard radar: A case study in modern incoherent scatter radar system design, *Radio Science*, 32, 2283–2307, <https://doi.org/10.1029/97RS01803>, 1997.
- Zettergren, M., Semeter, J., Burnett, B., Oliver, W., Heinselman, C., Brelly, P. L., and Diaz, M.: Dynamic variability in F-region ionospheric composition at auroral arc boundaries, *Annales Geophysicae*, 28, 651–664, <https://doi.org/10.5194/angeo-28-651-2010>, 2010.
- 290 Zettergren, M., Semeter, J., Heinselman, C., and Diaz, M.: Incoherent scatter radar estimation of F region ionospheric composition during frictional heating events, *Journal of Geophysical Research (Space Physics)*, 116, A01318, <https://doi.org/10.1029/2010JA016035>, 2011.